Journal of Materials Chemistry C

PAPER

View Article Online
View Journal | View Issue

Cite this: J. Mater. Chem. C, 2014, 2, 4799

Eu(II) luminescence in the perovskite host lattices $KMgH_3$, $NaMgH_3$ and mixed crystals $LiBa_xSr_{1-x}H_3$†

N. Kunkel,*[a] A. Meijerink,[b] M. Springborg[ac] and H. Kohlmann*[d]

Received 30th March 2014
Accepted 25th April 2014

DOI: 10.1039/c4tc00644e

www.rsc.org/MaterialsC

Bright luminescence of Eu(II) doped into the cubic perovskites $KMgH_3$ and mixed crystal compounds $LiBa_xSr_{1-x}H_3$ was observed and assigned to the $4f^65d–4f^7$ emission of Eu^{2+}. $KMgH_3$:Eu^{2+} shows an extremely bright yellow emission, whereas the wavelength of the emission maximum in $LiBa_xSr_{1-x}H_3$:Eu^{2+} depends on the value of x and ranges from yellow to green. Furthermore, an extremely wide red shift in the emission energy is observed for the orthorhombically distorted perovskite $NaMgH_3$:Eu^{2+}. Additionally, we review the crystal structure of $KMgH_3$ using density functional calculations.

Introduction

Eu(II) doped luminescent materials often show high luminescence efficiency and are therefore of great interest for applications as phosphors. To begin with, the transition between the $4f^65d$ and $4f^7$ levels of Eu(II) is a spin- and parity-allowed electric dipole transition. Furthermore, the emission energies depend strongly on the coordination sphere,[1] since the d levels are shielded only insufficiently against the lattice. Therefore, it is possible to affect the emission wavelength with the choice of the host lattice. Typically, blue or green emissions are observed in *e.g.* oxides or halides. In contrast, host lattices with more polarizable anions such as nitrides show a red shift in their emission energies and thus find application in efficient warm white LEDs.[2] Metal hydrides, which are well-known in the context of hydrogen storage materials,[3] can serve as interesting host lattices for Eu(II) luminescence. The hydride ligand is extremely polarizable, a fact that manifests itself in the extremely wide range of crystal radii known for hydride in different compounds.[4] The high polarizability and covalence is expected to strongly influence the position of the d-levels and thus the emission energies. A red emission was found for the alkaline earth metal hydrides of Ca, Sr and Ba[5] and the inverse cubic perovskites $LiMH_3$ (M = Sr, Ba)[6] also showed a considerable red shift compared to the emission of the isotypic fluoride compound $LiBaF_3$,[7] which was mainly explained by the strong nephelauxetic effect.

Within this work we studied Eu(II) luminescence in the perovskite-type compounds $KMgH_3$, $NaMgH_3$ and $LiBa_xSr_{1-x}H_3$. $KMgH_3$ has been prepared before[8,9] and was assumed to be isotypic to the fluoride compound $KMgF_3$ which crystallizes in the cubic perovskite structure type (see Fig. 1). However, unambiguous structure determination using neutron diffraction has not been carried out to the best of our knowledge. In the fluoride compound, ^6I emission of Eu^{2+} was observed[10] and explained by the small crystal field splitting and the high energetic position of the barycenter of the 5d levels. It was also shown spectroscopically from analysis of the number of Stark components of the f–f transition and symmetry analysis that Eu(II) occupies the monovalent K^+-site.[11,12] $NaMgH_3$ crystallizes in an orthorhombically distorted perovskite structure in

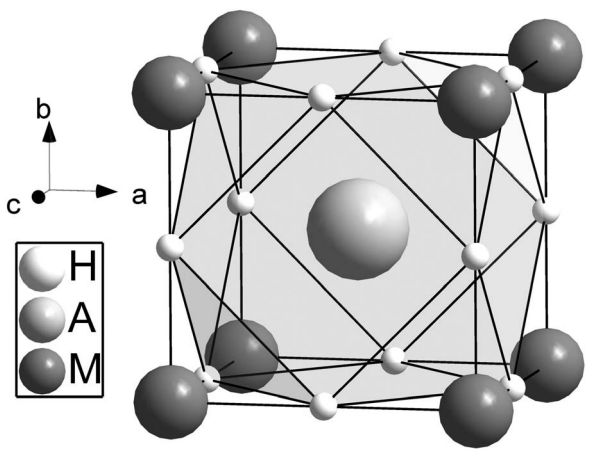

Fig. 1 The crystal structure of cubic perovskite type AMH_3 (*e.g.* A = K, M = Mg) showing the cuboctahedral surroundings of an A site with hydrogen. For $LiMH_3$ the cation sites are inverted, *i.e.* the M (*e.g.* Sr, Ba) atoms occupy the cuboctahedral positions.

[a]FR 8.1 Saarland University, P. O. Box 151150, 66041 Saarbrücken, Germany. E-mail: n.kunkel@mx.uni-saarland.de

[b]Debye Institute, Utrecht University, P. O. Box 80 000, 3508 TA Utrecht, The Netherlands

[c]School of Materials Science and Engineering, Tianjin University, Tianjin, 300072, People's Republic of China

[d]Leipzig University, Johannisallee 29, 04103 Leipzig, Germany. E-mail: holger.kohlmann@uni-leipzig.de

† Electronic supplementary information (ESI) available: Experimental details and additional luminescence spectra. See DOI: 10.1039/c4tc00644e

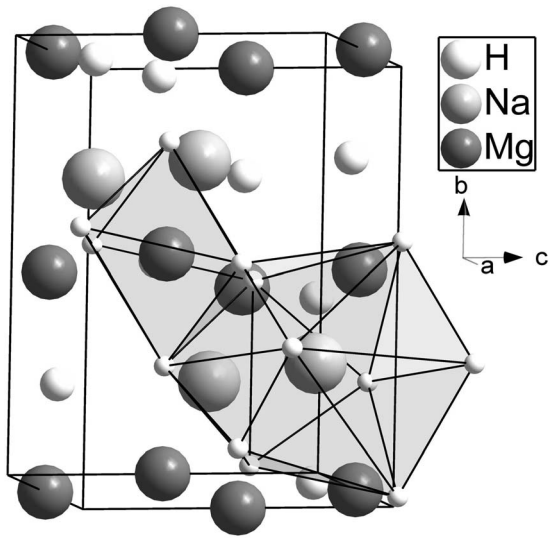

Fig. 2 The crystal structure of the orthorhombic perovskite $NaMgH_3$ in the $GdFeO_3$ type structure according to ref. 13.

the space group *Pnma* (see Fig. 2) isotypic to $GdFeO_3$.[13] In the closely related fluoride compound $NaMgF_3$ a strong 4f–4f line emission and a weak 5d–4f band emission in the ultraviolet were observed.[12,14] Analysis of the Stark components of the f–f transition also indicated that Eu^{2+} is located at the Na^+ site.[11]

The mixed crystals $LiBa_xSr_{1-x}H_3:Eu^{2+}$ crystallize in the inverse cubic perovskite type, which has been shown before for the end members of the series using neutron diffraction.[6,15]

In contrast to Eu^{2+} luminescence in fluoride host lattices crystallizing in the perovskite structure type,[7,10] the only hydrides that have been investigated so far are $LiMH_3$ (M = Sr, Ba).[6] Our present studies aim at investigating further examples of hydridic perovskites as host lattices for Eu^{2+} luminescence, in order to gain a more systematic classification.

Experimental

Materials and methods

$NaMgH_3$, $NaMgH_3:Eu^{2+}$, $KMgH_3$ and $KMgH_3:Eu^{2+}$ were prepared from NaH (Sigma Aldrich, 95%), KH (Sigma Aldrich, 50 wt% in paraffin, washed several times in hexane), fine magnesium powder (ABCR, 99.8%, under argon) and EuH_2 (prepared by hydrogenation of Eu ingot, 99.9% Alfa Aesar) in an autoclave consisting of the hydrogen resistant Nicrofer® 5219 alloy (*Inconel* 718) at approx. 780 K and 80–100 bar hydrogen pressure (reaction time 4 days). The alloys $LiBa_xSr_{1-x}:Eu^{2+}$ (M = Sr, Ba) were prepared by melting reactions of the elements (Eu ingots, 99.9%, Alfa Aesar; Sr pieces, 99.8%, Alfa Aesar; Ba pieces, 99.9%, Sigma Aldrich or barium rod, Chempur, 99.3% (rest strontium); all mechanically surface cleaned before use) in Nb ampoules and hydrogenated at 600 K and 80–150 bar H_2 pressure (H_2 99.9%) for approx. 3 days.

Due to moisture and air-sensitivity, all utilized hydrides, metals and alloys were handled in an argon-filled glove box. Since the products are ionic hydrides, they are relatively stable against temperature if handled under an inert gas or hydrogen atmosphere. $LiBa_xSr_{1-x}H_3$ are stable up to at least 450 °C, whereas $KMgH_3$ and $NaMgH_3$ are stable up to approximately 300 °C. Higher temperature stabilities are obtained using elevated hydrogen pressures.

Structures were characterized *via* X-ray powder diffraction (for details see ESI†).

Photoluminescence emission and absorption spectra were measured on an Edinburgh Instruments FLS920 spectrofluorometer equipped with a double monochromator according to Czerny–Turner (300 mm focal length) for the excitation beam, a monochromator for UV/vis detection, a 450 W xenon lamp for sample excitation and a photomultiplier tube R928P (Hamamatsu) for detection. Measurements at low temperatures were carried out using an Oxford liquid helium flow cryostat. If not indicated otherwise, spectra were corrected for lamp intensity and photomultiplier sensitivity. Luminescence decay curves were measured under pulsed excitation with an Edinburgh 376.8 nm pulsed diode laser with 65 ps pulses. Due to moisture and air sensitivity, samples were enclosed in sealed silica tubes of 0.5–1 cm diameter. A single exponential function was used for analysis of the luminescence decay curves, neglecting the small deviation from single exponential within the higher temperature range (faster initial decay).

Electronic structure calculations of $KMgH_3$ in the normal and inverse cubic perovskite structure type were performed using the Vienna *ab initio* simulation package (VASP)[16,17] together with PAWs.[18] Exchange-correlation effects were treated with the generalized gradient approximation of Perdew and Wang[19] and evaluation of the electronic properties was carried out using the tetrahedron method with Blöchl corrections.[20] Brillouin zone integration was performed over a Γ-centered 15 × 15 × 15 Monkhorst–Pack grid.[21] A cut-off of 600 eV was applied for the plane-wave expansion of the electronic orbitals, forces were converged to 0.1 meV $Å^{-1}$ and the criterion for electronic convergence was 0.01 meV. Potential curves were evaluated using VASP within the ASE atomic simulation environment.[22]

Results and discussion

$KMgH_3:Eu^{2+}$

$KMgH_3:Eu^{2+}$ (1.0 mol% with respect to K) was obtained as a light grey powder and shows an exceptionally intense yellow emission under UV excitation (see Fig. 3).

DFT calculations show that the normal cubic perovskite structure type is energetically favored compared to the inverse cubic perovskite structure type (see Fig. 4). Calculated and experimentally determined unit cell volumes are in good agreement (Fig. 4 and Table 1).

In the normal cubic perovskite type $A^IM^{II}X_3$, M is octahedrally coordinated by six hydrogen atoms, whereas the coordination of A is a cuboctahedral arrangement of twelve hydrogen atoms. As the difference in radii for Mg^{2+} and Eu^{2+} is rather large, whereas the radius of Eu^{2+} is close to that of K^+,[23] europium is assumed to occupy the site of potassium which has the

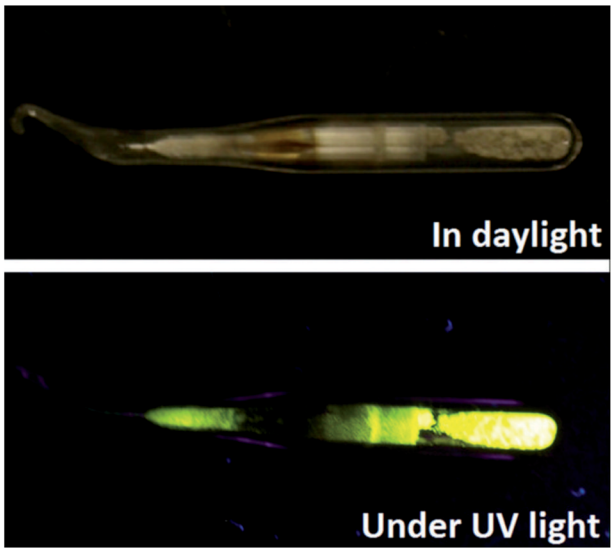

Fig. 3 $KMgH_3:Eu^{2+}$ (1.0 mol%) sealed in a silica ampoule in daylight (top) and under UV excitation (360 nm, bottom).

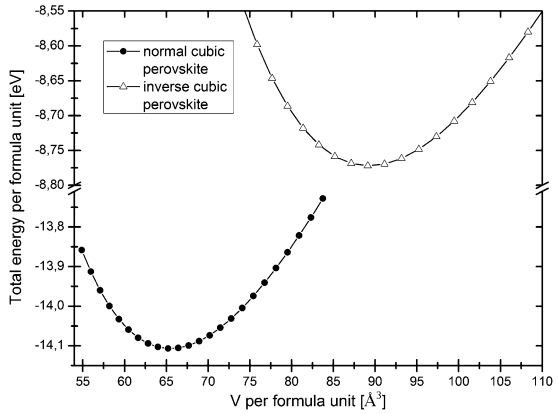

Fig. 4 Calculated potential curves for $KMgH_3$ in the normal and the inverse cubic perovskite structure type.

Table 1 Lattice parameters and interatomic distances in $KMgH_3:Eu^{2+}$ (1.0 mol%) (in pm) at 293(1) K. ($KMgH_3$ $a = 402.791(6)$)

$KMgH_3:Eu^{2+}$ $a = 403.179(7)$	
Eu/K–H	285.091(5)
Mg–H	201.589(4)

symmetry $m\bar{3}m$. This assumption is in agreement with the observation of Eu(II) on the K^+-site in $KMgF_3$.[11]

Assuming a statistical occupation of the potassium site by europium and potassium, the interatomic distances (listed in Table 1) are obtained from room temperature X-ray powder diffraction (XRPD) measurements.

Temperature dependent XRPD data of $KMgH_3$ from 20 to 200 K also show that a phase transition at low temperature can be excluded (see Fig. 1 of the ESI†). The temperature dependent lattice constants are listed in Table 2. Between 20 and 200 K the

Table 2 Temperature dependence of the lattice constant a (pm) in $KMgH_3$

T/K	a
20	400.95(2)
40	400.95(2)
60	401.00(2)
80	401.07(2)
100	401.16(1)
200	401.68(3)

temperature dependence can be described *via* polynomials of second order, $a(T) = a_0 + a_1T + a_2T^2$ with $a_0 = 400.90(2)$ pm, $a_1 = 0.0011(5)$ pm K^{-1} and $a_2 = 1.4(2) \times 10^{-5}$ pm K^{-2}. A linear regression of the lattice parameter a between 20 and 100 K yielded a coefficient for linear expansion of $7.4(9) \times 10^{-6}$ pm K^{-1}.

Luminescence spectra exhibit broad band emission and excitation bands which we assigned to the parity-allowed electric dipole transitions between the $4f^6$5d and the $4f^7$ levels of Eu(II). The emission maximum is at about 565 nm. In Fig. 5 temperature-dependent emission spectra are shown. With decreasing temperature, emission intensities increase significantly.

The replacement of K^+ by Eu^{2+} requires charge compensation. However, charge compensation by nearby K^+ vacancies will lead to different local environments around Eu^{2+} and lower the symmetry. The observation of a slightly unsymmetrical peak shape with a shoulder on the longer wavelength side indicates the presence of overlapping emission bands and thus different local environments around Eu^{2+}.

The strong increase in the emission intensities with decreasing temperature is in good agreement with the observation of a quenching temperature of approx. 240 K.

The temperature-dependence of the lifetimes and emission intensities are shown in Fig. 6 and the excitation spectrum at 4 K in Fig. 5 of the ESI.†

The small offset in the intensities between 150 and 170 K compared to the lifetimes is due to small fluctuations in

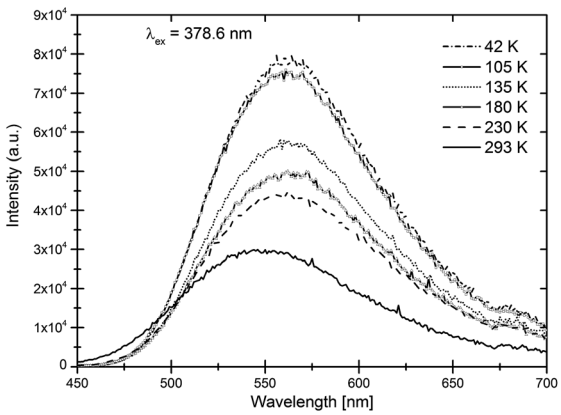

Fig. 5 Temperature-dependent luminescence spectra of $KMgH_3:Eu^{2+}$ (1.0 mol%).

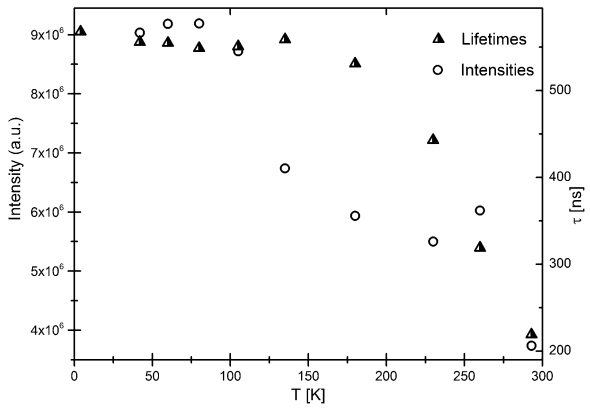

Fig. 6 Temperature dependence of the emission intensities and lifetimes of $KMgH_3$:Eu^{2+} (1.0 mol%).

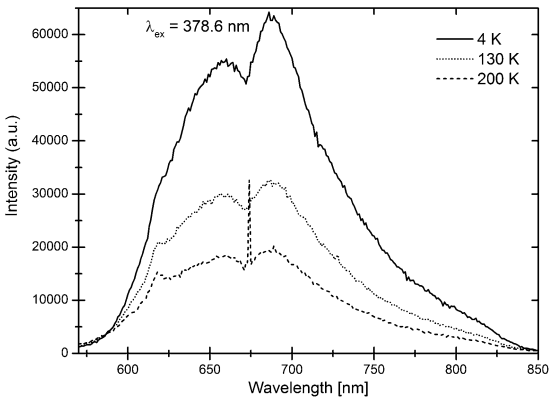

Fig. 7 Temperature-dependent luminescence emission spectra of $NaMgH_3$:Eu^{2+} (1.0 mol%).

temperature while heating and cooling the cryostat. No fine structures are visible at low temperatures, an observation which indicates a rather large Huang–Rhys coupling parameter. Lifetimes at low temperatures are approx. 700 ns, which is slightly smaller than the expected decay times of 1–1.4 μs for Eu^{2+} emission around 560 nm.[24] As discussed in ref. 6, the slightly shorter decay time might be caused by the higher refractive index *n* of hydrides compared to most oxides, which leads to an increase of the radiative decay rate.

$NaMgH_3$:Eu^{2+}

$NaMgH_3$:Eu^{2+} (1.0 mol% with respect to Na) was obtained as an orange powder and shows only a very weak red emission at room temperature. The hydride crystallizes in an orthorhombically distorted perovskite structure, where the coordination polyhedron around Na^+ is a bicapped distorted cube built up by hydride ligands and Mg^{2+} is located inside a distorted octahedron. Similar to the potassium compound, we assume Eu^{2+} to occupy the Na^+ site since the radii of Eu^{2+} and Mg^{2+} differ significantly and the radius of Na^+ is closer to Eu^{2+}.[23] This assumption was proven for the structurally related fluoride compound $NaMgF_3$.[11]

Assuming a statistical occupation of the sodium site by europium and sodium, the following average interatomic distances are obtained from room temperature XRPD measurements. Since several Mg–H and Na–H distances exist, average distances are given in parenthesis (Table 3).

With decreasing temperature the emission intensities increase significantly (see Fig. 7).

The observation of a second maximum at 700 nm in Fig. 7 might be an instrumental artefact due to variations in the detector response and monochromator through-put in this spectral range. $NaMgH_3$:Eu^{2+} (1.0 mol%) shows an emission at about 680 nm which is, next to Eu(II) luminescence in alkaline earth metal hydrides,[5] one of the widest redshifts for Eu(II) emission ever reported. The wide FWHM of the emission peak and the shoulder on the longer wavelength side might be due to the existence of slightly different local environments around Eu^{2+} which are caused by charge compensation. Even at 4 K, decay curves do not show a single exponential behavior and lifetimes are extremely short, indicating that the emission is still quenched to a large extent.

Table 3 Lattice parameters and interatomic distances in $NaMgH_3$:Eu^{2+} (1.0 mol%) (in pm) at 293(1) K. ($NaMgH_3$ $a = 546.340(9)$, $b = 770.36(1)$, $c = 541.351(9)$)

$NaMgH_3$:Eu^{2+} $a = 546.85(1)$, $b = 771.12(2)$, $c = 541.92(1)$	
Eu/Na–H	227.368(5)–300.820(5) (av. 263.311(5))
Mg–H	196.148(5)–197.877(5) (av. 197.110(5))

$LiBa_xSr_{1-x}H_3$:Eu^{2+}

Compounds of the system $LiBa_xSr_{1-x}H_3$:Eu^{2+} (0.5 mol% with respect to Sr/Ba) were obtained as light yellow powders, and emit, depending on the value of *x*, yellow to green light under UV excitation. Since $LiEuH_3$ crystallizes in the inverse cubic perovskite type, too,[25,26] Eu^{2+} is assumed to occupy the high-symmetry site ($m\bar{3}m$) of Sr^{2+} or Ba^{2+} and is thus twelve-fold coordinated by hydride. Pure samples were obtained only for $x \leq 0.35$ and ≥ 0.89. In between these regions, mixtures of

Table 4 Nominal compositions in $LiBa_xSr_{1-x}H_3$:Eu^{2+} (0.5 mol%), nr. of cubic perovskite phases found, refined lattice parameters, mean strain value ε_0, maximum emission wavelengths and FWHM of the emission bands

x	nr. of phases	*a* [pm]/ε_0	λ_{em} [nm]/FWHM [nm]
0.0	1	383.498(3)/0.049(7)	580(98)
0.193	1	387.536(4)/0.169(3)	581(105)
0.298	1	389.81(2)/0.250(5)	579(105)
0.351	1	391.21(1)/0.23(1)	582(108)
0.492	3	401.02(1)/0.15(2)	560(107)
		396.98(1)/0.57(2)	
		385.15(1)/0.17(5)	
0.642	3	401.62(1)/0.121(9)	565(113)
		398.5(1)/0.37(3)	
		386.68(4)/0.09(1)	
0.89	1	401.250(3)/0.107(2)	533(88)
1.0	1	402.284(3)/0.035(1)	524(87)

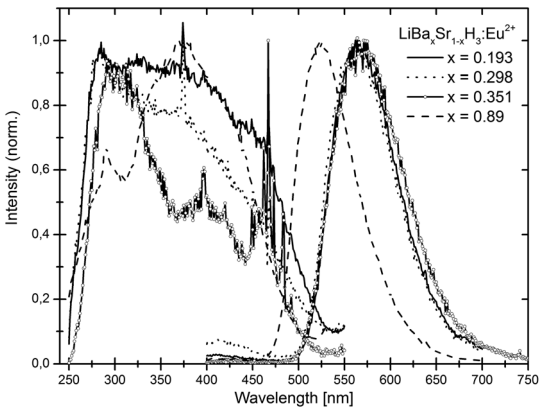

Fig. 8 Luminescence excitation (left) and emission spectra (right) of $LiBa_xSr_{1-x}H_3:Eu^{2+}$ (0.5 mol%) at room temperature.

perovskite phases were obtained. Higher reaction temperatures (tested up to 780 K) did not yield single phase samples either. The nominal values for x, the numbers of phases found, the lattice parameter a, ε_0 as a measure of strain, the emission maxima and the full width at half maximum (FWHM) of the emission bands are given in Table 4.

Luminescence properties of the end members are described in ref. 6 and will therefore not be discussed here any further. It is remarkable that the mean strain value ε_0, as well as the FWHM of the emission band, have their highest values for the samples with several perovskite phases. In these multiphase mixtures, the strain is largest for those phases with intermediate lattice parameters. This is in accordance with the assumption of a solid solution series, in which the maximum of the micro strain is expected for a strontium to barium ratio around one.

Room temperature luminescence emission spectra for the pure samples with $x = 0.193$, 0.298, 0.351 and 0.89 are shown in Fig. 8.

Up to $x = 0.351$ almost no change in the emission maximum is observed compared to $LiSrH_3:Eu^{2+}$, indicating a preferred occupation of a strontium-rich environment by Eu^{2+}.

Comparison of the emission energies of the $4f^65d$–$4f^7$ transition of Eu(II) in metal hydrides

In Table 5 a comparison of the emission energies of the $4f^65d$ states of Eu(II), coordination polyhedra and interatomic distances in different hydride host lattices is given [(ref. 5 and 6), this work]. Possible local distortions caused by europium are ignored. Interatomic distances are given for doping concentrations ≤1 mol%.

Generally, as already shown in ref. 6, Eu^{2+} emission energies in hydride host lattices are shifted to longer wavelengths compared to similar fluoride host lattices. This shift is mainly caused by the strong nephelauxetic effect of the hydride ligand. A decrease in the interatomic Eu–H distance leads to a shift to longer wavelengths, except for BaH_2 and $KMgH_3$. For BaH_2 anomalous emission was given as an explanation.[5] In $KMgH_3$ the emission wavelength is slightly longer than expected based on the comparison of interatomic distances. However, here Eu(II) is presumed to occupy a monovalent lattice site whereas for all other lattices except $NaMgH_3$ an occupation of a divalent lattice site is expected. Possible charge compensations in $KMgH_3$ caused by Eu^{2+} doping may lead to local distortions that are not considered here. Equivalent to $KMgH_3$, local distortions in $NaMgH_3$ may be the reason for the observation of the extremely long emission wavelength and the low quenching temperature. Clearly, further investigations are necessary, in order to evaluate and extend the preliminary conclusions of factors governing Eu(II) based luminescence in metal hydrides drawn here.

Conclusions

Due to the large polarizability of the hydride ligand, salt-like metal hydrides form an interesting new class of host lattices for Eu^{2+} luminescence. Within this work we observed bright yellow and green luminescence for $KMgH_3$ and $LiBa_xSr_{1-x}H_3$ and red emission in $NaMgH_3$ under UV excitation. Thus the substitution of fluoride by hydride in $KMgH_3$ and $NaMgH_3$ leads to an exceptionally large shift to longer emission wavelengths, which can be explained by the strong nephelauxetic effect and the larger ligand field splitting of hydride. Such host lattices with emission wavelengths in the yellow or red color region might be of interest for warm-light-emitting LEDs, even though a contact of the phosphor with air would need to be prevented by the use of a suited encapsulation. $KMgH_3$ crystallizes in the normal cubic perovskite type according to quantum chemical calculations. Eu(II) is assumed to be placed on the site of potassium, which introduces different environments due to charge

Table 5 Comparison of the emission energies of the $4f^65d$ states of Eu(II) in different hydride host lattices and coordination environments of Eu(II) (data from ref. 5 and 6, this work). The assumed occupation site is given in parenthesis

Compound	Emission onset (nm)	Emission max. (nm)	Coordination nr., polyhedron and Eu–H distance (pm) (av. (pm))
$LiBaD_3$(Ba)	483	528	Cuboctahedron (CN 12), 283.7
$LiBaH_3$(Ba)	485	530	Cuboctahedron (CN 12), 284.5
$LiSrD_3$(Sr)	528	575	Cuboctahedron (CN 12), 270.5
$LiSrH_3$(Sr)	530	565	Cuboctahedron (CN 12), 271.2
$KMgH_3$(K)	538	565	Cuboctahedron (CN 12), 285.1
$NaMgH_3$(Na)	580	680	Dicapped distorted cube (CN 10), 227.4–300.8 (263.3)
SrH_2	637	728	Distorted tricapped trigonal prism (CN 9), 234–284 (260)
BaH_2	603	765	Distorted tricapped trigonal prism (CN 9), 254–296 (279)
CaH_2	670	765	Distorted tricapped trigonal prism (CN 9), 205–270 (234)

compensation in the neighbourhood and thus unsymmetrical peak shapes in luminescence spectra. The radiative lifetime of Eu^{2+} in $KMgH_3$ is 700 ns which is slightly shorter than observed for halide and oxide host lattices and might be explained by the higher refractive index of hydrides. For $NaMgH_3$:Eu^{2+}, which shows an extreme red shift of the Eu(II) emission to about 680 nm, extremely short lifetimes are observed, suggesting that the luminescence is partly quenched even at low temperatures. Even though no complete solution series was found for $LiBa_xSr_{1-x}H_3$, substitution of strontium by barium in the regions of complete miscibility led to a shift in the emission wavelength. In general, an occupation of a strontium-rich local environment by Eu^{2+} seems to be preferred, which is not unexpected given the similar ionic radii of Sr^{2+} and Eu^{2+}. Those results confirm the observation of a large shift to longer wavelengths of Eu^{2+} $4f^65d$ emission in hydride host lattices caused by the strong nephelauxetic effect of the hydride ligand and help understanding of the class of metal hydride host lattices for Eu^{2+} luminescence.

Acknowledgements

We are grateful to the Landesgraduiertenförderung Saar for a PhD research fellowship and the Deutsche Forschungsgemeinschaft (DFG) for financial support (grants KO1803/3-1 and KO1803/7-1). We also thank Wenjie Yan and PD Dr Richard Weihrich for temperature-dependent XRD measurements of $KMgH_3$. Furthermore, one of us wants to thank Dr Robert Haberkorn for insightful discussions.

Notes and references

1 P. Dorenbos, *J. Lumin.*, 2003, **104**, 239.
2 H. A. Höppe, *Angew. Chem., Int. Ed.*, 2009, **48**, 3572.
3 U. Eberle, M. Felderhoff and F. Schüth, *Angew. Chem.*, 2009, **121**, 6732.
4 D. F. C. Morris and G. L. Reed, *J. Inorg. Nucl. Chem.*, 1965, **27**, 1715.
5 N. Kunkel, H. Kohlmann, A. Sayede and M. Springborg, *Inorg. Chem.*, 2011, **50**, 5873.
6 N. Kunkel, A. Meijerink and H. Kohlmann, *Phys. Chem. Chem. Phys.*, 2014, **16**, 4807.
7 A. Meijerink, *J. Lumin.*, 1993, **55**, 125.
8 E. C. Ashby, R. Kovar and R. Arnott, *J. Am. Chem. Soc.*, 1970, **92**, 2182–2183.
9 R. Schumacher and A. Weiss, *J. Less-Common Met.*, 1990, **163**, 179.
10 A. Ellens, A. Meijerink and G. Blasse, *J. Lumin.*, 1994, **59**, 293.
11 N. S. Altshuler, L. D. Livanova and A. L. Stolov, *Opt. Spectrosc.*, 1974, **36**, 72.
12 S. N. Bodrug, E. G. Valyashko, V. N. Mednikova, D. T. Sviridov and R. K. Sviridov, *Opt. Spectrosc.*, 1973, **34**, 176.
13 E. Rönnebro, D. Noréus, K. Kadir, A. Reiser and B. Bogdanovic, *J. Alloys Compd.*, 2000, **299**, 101.
14 J. L. Sommerdijk and A. Bril, *J. Lumin.*, 1976, **11**, 363.
15 A. J. Maeland and A. F. Andresen, *J. Chem. Phys.*, 1968, **48**, 4660.
16 G. Kresse and J. Furthmüller, *Phys. Rev. B: Condens. Matter Mater. Phys.*, 1996, **54**, 11169.
17 J. Hafner, *J. Comput. Chem.*, 2008, **29**, 2044.
18 P. E. Blöchl, *Phys. Rev. B: Condens. Matter Mater. Phys.*, 1994, **50**, 17953.
19 J. P. Perdew and Y. Wang, *Phys. Rev. B: Condens. Matter Mater. Phys.*, 1992, **45**, 13244.
20 P. E. Blöchl, O. Jepsen and O. K. Andersen, *Phys. Rev. B: Condens. Matter Mater. Phys.*, 1994, **49**, 16232.
21 H. J. Monkhorst and J. D. Pack, *Phys. Rev. B: Condens. Matter Mater. Phys.*, 1976, **13**, 5188.
22 S. R. Bahn and K. W. Jacobsen, *Comput. Sci. Eng.*, 2002, **4**, 56.
23 R. D. Shannon, *Acta Crystallogr., Sect. A: Found. Crystallogr.*, 1976, **32**, 751.
24 S. H. M. Poort, A. Meijerink and G. Blasse, *J. Phys. Chem. Solids*, 1997, **58**, 1451.
25 H. Kohlmann and K. Yvon, *J. Alloys Compd.*, 2000, **299**, L16.
26 B. Blaschkowski, M. Kaller and T. Schleid, *Z. Anorg. Allg. Chem.*, 2006, **632**, 2149.